

# Reversible Methanolation of Metal Halide Perovskites

Bryan A. Rosales, Laura E. Mundt, Laura T. Schelhas, and Lance M. Wheeler\*



Cite This: <https://doi.org/10.1021/jacs.1c10942>



Read Online

ACCESS |



Metrics & More



Article Recommendations



Supporting Information

**ABSTRACT:** The low formation energies inherent in metal halide perovskites enable the structure to be easily broken and remade with little energy input. In this work, we leverage low formation energy to demonstrate 0D/3D structural transformations induced by reversible intercalation of methanol to yield dramatic control of visible light absorption. We identify a methanolated structure that features sheets of 0D isolated  $[\text{PbI}_6]^{4-}$  octahedra separated by MAI and methanol. Methanol and water reversibly displace each other in the 0D complex by controlling the chemical potential of the system via Le Chatelier's principle. The weaker H-bonding of methanol compared to water effectively reduces the complex dissociation temperature from 70 to 50 °C, rendering the methanol complex more desirable for an array of next-generation applications spanning low-power-consumption memory to switchable photovoltaics.

Metal halide perovskite (MHP) materials are an exciting class of optoelectronic semiconductors<sup>1–6</sup> that exhibit a soft ionic lattice resulting in crystalline-like electronic band structures with liquid-like physical properties.<sup>7</sup> The presence of low formation energies allows MHPs to be fabricated from solution under mild conditions with little energy input.<sup>8</sup> However, these low formation energies also lead to detrimental properties such as facile ion migration and decomposition or transformation to undesired phases upon exposure to a variety of stimuli such as humidity, heat, and light.<sup>9</sup> Despite these challenges, MHPs have been developed for an array of optoelectronic applications, including solar cells with record power conversion efficiencies (PCEs) exceeding 25%.<sup>10</sup>

The small lattice energy of MHPs allows reversible structural transformations by accommodating a variety of intercalation species at standard conditions. Molecules are intercalated into the MHP structure by interacting favorably with the lattice through the formation of hydrogen,<sup>11–13</sup> charge-transfer,<sup>14–17</sup> ionic,<sup>18</sup> van der Waals,<sup>19</sup> and  $\pi$ -stacked fluorylaryl–aryl bonds.<sup>20</sup> Complex formation and dissociation can be controlled by modulating the strength of interactions between the intercalating molecule and the MHP lattice.

The most investigated complexes are those based on H-bonding.<sup>11–13,21–26</sup> H-bonds formed between intercalating molecules and the MHP lattice are strong enough to form stable complexes at room temperature yet weak enough to easily dissociate upon heating. Tuning the complex bonding strength results in structural transformations that occur in seconds to minutes<sup>11,12,21,22</sup> compared to phase transformations between  $\alpha$  and  $\delta$  phases that occur over several hours.<sup>27</sup> The strong H-bonding nature of methylammonium (MA) is critical for complex formation. Weaker H-bonding cations like Cs and formamidinium have not been shown to form stable intercalation complexes with vapor. Exposure of  $\text{MAPbI}_3$  films to methylamine ( $\text{CH}_3\text{NH}_2$ ) vapor forms the complex  $\text{MAPbI}_3 \cdot x\text{CH}_3\text{NH}_2$  dissociated at temperatures above 60 °C. Photovoltaic windows fabricated from the  $\text{MAPbI}_3 \cdot$

$x\text{CH}_3\text{NH}_2$  complex switch between a colored phase and a bleached phase where the colored phase shows a PCE as high as 11.3%.<sup>12</sup>  $\text{H}_2\text{O}$  cointercalates with MAI into  $\text{MAPbI}_3$  at relative humidity >40% to form  $\text{MA}_4\text{PbI}_6 \cdot 2\text{H}_2\text{O}$ ,<sup>13,21–26</sup> which is dehydrated to reform  $\text{MAPbI}_3$  at 75 °C.<sup>22</sup>

MeOH has long been used in MHP fabrication as an antisolvent to form both films<sup>28</sup> and powders,<sup>29</sup> as a solvent to remove excess AX (A = monovalent cation) salts,<sup>30</sup> and for vapor annealing to promote grain growth.<sup>31</sup> Herein, we show that MeOH reversibly cointercalates with MAI molecules into the 3D  $\text{MAPbI}_3$  MHP structure to form the 0D  $\text{MA}_6\text{PbI}_8 \cdot 2\text{MeOH}$  complex. We also show that MeOH and  $\text{H}_2\text{O}$  reversibly displace each other from the MHP lattice via Le Chatelier's principle upon exposure to an excess of the opposite vapor. MeOH forms weaker H-bonds with the MHP lattice than  $\text{H}_2\text{O}$ , resulting in a reduced complex dissociation temperature. Low-energy modulation of the semiconductor properties will underpin applications such as low-power-consumption memory, neuromorphic computing, switchable photovoltaics, and thermochromic windows.

We fabricate switchable MHP films by spin-coating a solution of 4:1 MAI:PbI<sub>2</sub> under inert conditions (see Experimental Details in the Supporting Information). The visual appearance of initial films is reddish-brown (Figure 1a). Exposure to  $\text{H}_2\text{O}$  or MeOH vapor induces a rapid structural transformation that results in a transparent, colorless film within <2 min. The film is regenerated to the original reddish-brown color by gently heating hydrated and methanolated films at 70 or 50 °C, respectively (Figure 1a and Figure S1). These observations suggest that an intercalation complex is

Received: October 15, 2021

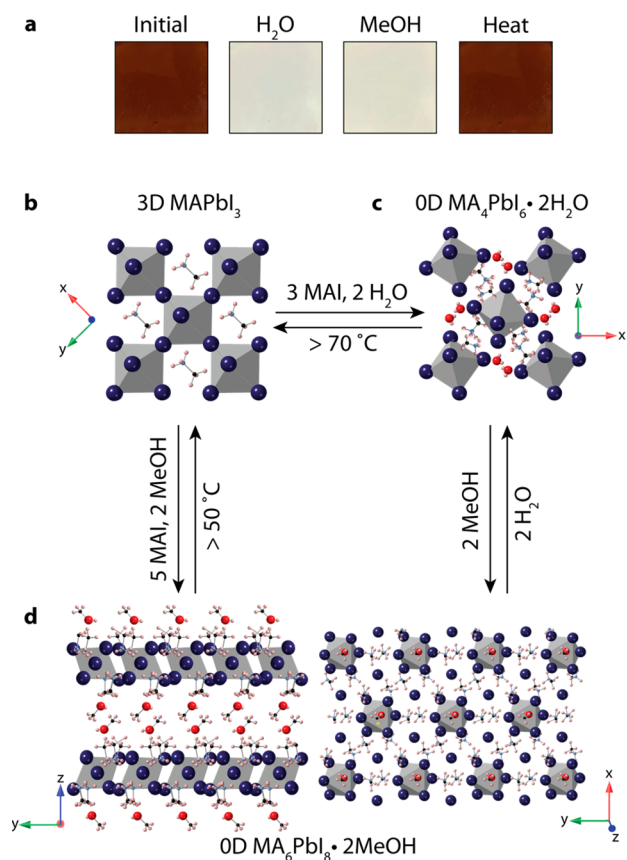


**Figure 1.** (a) Photographs showing the color change of the same switchable MHP film exposed to H<sub>2</sub>O, MeOH, and heat. Illustration comparing the crystal structures of (b) 3D MAPbI<sub>3</sub>, (c) 0D MA<sub>4</sub>PbI<sub>6</sub>·2H<sub>2</sub>O hydrate complex, and (d) 0D MA<sub>6</sub>PbI<sub>8</sub>·2MeOH methanolate complex.

formed that requires overcoming a minimum thermal energy threshold for complex dissociation.

Attenuated total reflection Fourier transform infrared (ATR-FTIR) spectroscopy confirms that H<sub>2</sub>O and MeOH are incorporated into the film upon exposure to vapor and removed after heating (Figure S2 and Table S1). Prior reports show that MHPs reversibly form 0D complexes with H<sub>2</sub>O;<sup>13,21,22</sup> however, there are no known reports of complex formation with alcohols. Other alcohols like ethanol (EtOH) and isopropyl alcohol (IPA) do not induce color change. We hypothesize EtOH and IPA are too large to fit into the MHP structure, and the H-bonding strength is too weak to form a complex at standard conditions.

We attribute the mechanism of color change to an equilibrium between 0D complex formation with H<sub>2</sub>O or MeOH vapor (bleached state) and complex dissociation into 3D MAPbI<sub>3</sub> (Figure 1b) nanocrystals embedded within an excess MAI matrix upon heating (colored state). Complex formation and dissociation are dictated by H-bond interactions between the intercalating molecule and the MHP lattice. The MeOH complex dissociates at lower temperatures (50 °C) than the H<sub>2</sub>O complex (70 °C), which suggests that MeOH forms weaker H-bonds with the MHP lattice.

Unlike switchable MHP films exposed to H<sub>2</sub>O that form the 0D MA<sub>4</sub>PbI<sub>6</sub>·2H<sub>2</sub>O hydrate complex (Figure 1c), the weaker H-bonding of MeOH causes films to form a 0D MA<sub>6</sub>PbI<sub>8</sub>·2MeOH structure that is richer in MAI (Figure 1d). We

simulated MA<sub>6</sub>PbI<sub>8</sub>·2MeOH from the crystal structure of PEA<sub>6</sub>SnBr<sub>8</sub>·2CCl<sub>2</sub>H<sub>2</sub> (PEA = phenethylammonium)<sup>33</sup> by modifying elemental composition and maintaining the monoclinic *Cc* space group. Our best fit after Rietveld refinement was obtained with  $a = 13.495812 \text{ \AA}$ ,  $b = 7.758366 \text{ \AA}$ ,  $c = 20.429327 \text{ \AA}$ ,  $\alpha = \gamma = 90^\circ$ , and  $\beta = 102.76711^\circ$ . The structure of the 0D MA<sub>6</sub>PbI<sub>8</sub>·2MeOH complex forms sheets of isolated [PbI<sub>6</sub>]<sup>4-</sup> octahedra that allow the larger MeOH molecule to occupy the space between sheets whereas the 0D MA<sub>4</sub>PbI<sub>6</sub>·2H<sub>2</sub>O hydrate complex forms an isotropic network of hydrated [PbI<sub>6</sub>]<sup>4-</sup> octahedra.

The 0D methanolated MHP structure was identified by *in situ* wide-angle X-ray scattering (WAXS). Reddish-brown films show expected Bragg diffraction peaks of 3D MAPbI<sub>3</sub> and MAI (Figure 2a and Figure S3a). All 3D MAPbI<sub>3</sub> peaks disappear, and MAI peaks decrease in intensity over the course of 90 s after exposure to MeOH. New peaks emerge between 45 and 60 s corresponding to 0D MA<sub>6</sub>PbI<sub>8</sub>·2MeOH with intensity increasing until 2 min 45 s. Diffraction peaks from an unknown phase associated with methanolation also emerge between 45 and 60 s, but growth occurs faster with maximum scattering intensity occurring after 1 min 30 s.

Annealing above 50 °C initiates complex dissociation: first by the disappearance of 0D MA<sub>4</sub>PbI<sub>6</sub>·2MeOH over 1 min 45 s, followed by the disappearance of the unknown phase over 5 min. The 3D MAPbI<sub>3</sub> peaks simultaneously re-emerge over 2 min 45 s. Scherrer analysis performed on the (100) peak of 3D MAPbI<sub>3</sub> indicates that the single crystalline domain size is maintained with values of  $36 \pm 3 \text{ nm}$  before complex formation and  $37 \pm 4 \text{ nm}$  after complex dissociation (Figure 2c). The Scherrer size of 0D MA<sub>6</sub>PbI<sub>8</sub>·2MeOH and the unknown phase is larger than that of the 3D MAPbI<sub>3</sub> phase, which suggests that larger domains are formed by incorporation of the adjacent MAI phase into the 3D MAPbI<sub>3</sub> domains. Formation of the unknown phase before 0D MA<sub>6</sub>PbI<sub>8</sub>·2MeOH and dissociation of the unknown phase after 0D MA<sub>6</sub>PbI<sub>8</sub>·2MeOH suggests that the unknown phase is likely a structural intermediate between 3D MAPbI<sub>3</sub> and 0D MA<sub>6</sub>PbI<sub>8</sub>·2MeOH that stabilizes the 0D MA<sub>6</sub>PbI<sub>8</sub>·2MeOH structure and balances the stoichiometry of the excess MAI.

We attempted to identify the unknown phase. The intensity and FWHM evolution of the unknown peaks suggest it is a single phase independent from 0D MA<sub>6</sub>PbI<sub>8</sub>·2MeOH (Figure 2b,c). The methanolated film also contains peaks corresponding to crystalline MAI, which suggests the unknown phase does not form in a 1:1 ratio and is likely poorer in MAI and richer in PbI<sub>2</sub> relative to the 0D MA<sub>6</sub>PbI<sub>8</sub>·2MeOH phase. The 1D diffraction patterns were fit to various known polymorphs of low-dimensional MHP phases such as APb<sub>2</sub>I<sub>5</sub>, A<sub>2</sub>PbI<sub>4</sub>, A<sub>3</sub>PbI<sub>5</sub>, and A<sub>4</sub>PbI<sub>6</sub> with and without intercalating molecules, but we could not confirm the structure. We were also unsuccessful at growing single crystals of the 0D MA<sub>6</sub>PbI<sub>8</sub>·2MeOH compound or the unknown phase in order to resolve the crystal structure with single crystal X-ray diffraction.

Switchable MHP films are readily interconverted between methanolated and hydrated complexes by changing the chemical potential of the system through Le Chatelier's principle. *In situ* WAXS shows that exposing a methanolated film to H<sub>2</sub>O vapor initiates a rapid transformation from 0D MA<sub>6</sub>PbI<sub>8</sub>·2MeOH and the unknown phase associated with methanolation to 0D MA<sub>4</sub>PbI<sub>6</sub>·2H<sub>2</sub>O in under 15 s (Figure 2d–f). This transformation is reversed at a slightly slower rate of 30 s by exposing the hydrated film to MeOH vapor. The

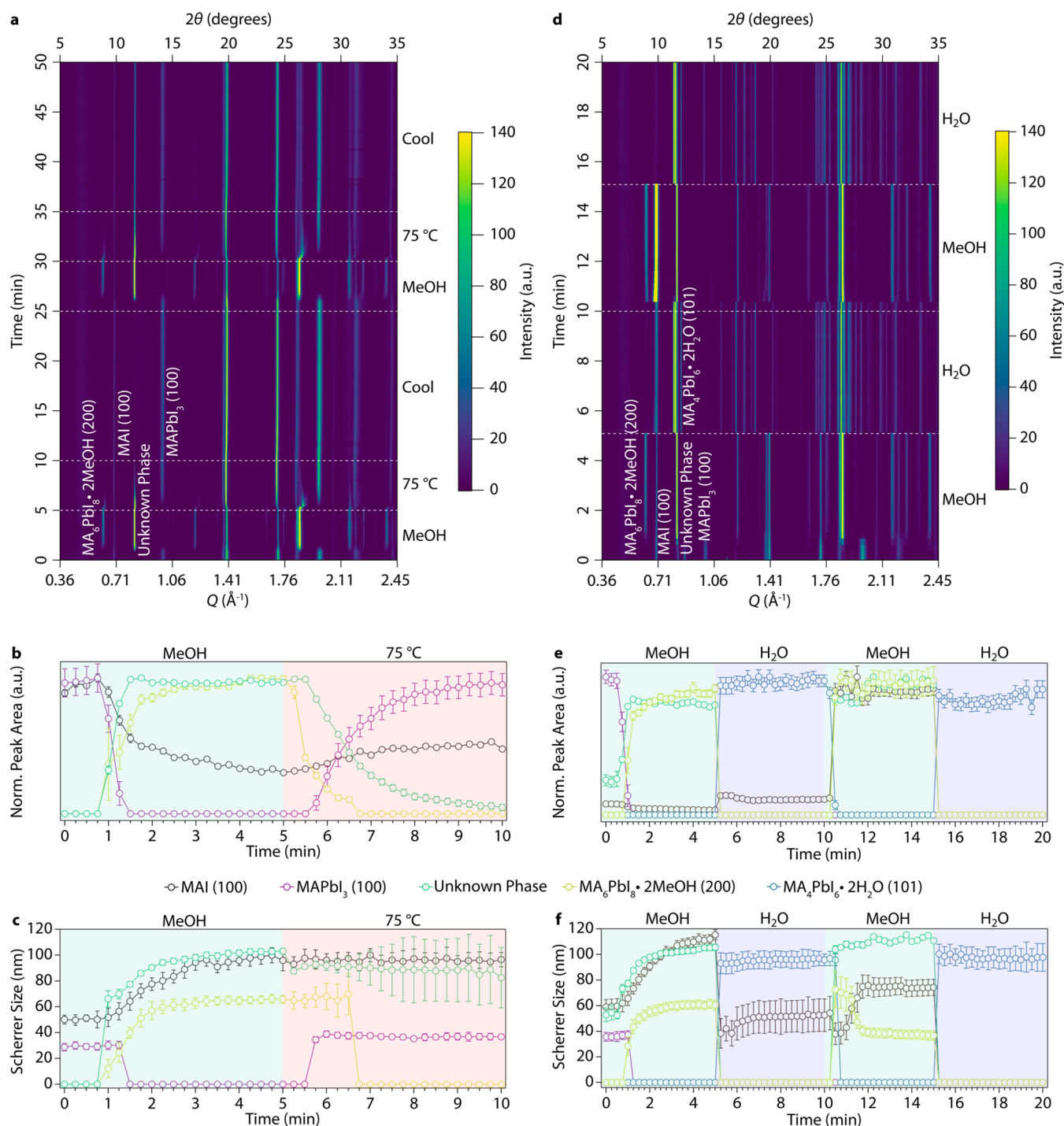


**Figure 2.** *In situ* WAXS data collected over (a) two cycles of alternating exposure to MeOH vapor and 75 °C. Comparison of MAI (100), MAPbI<sub>3</sub> (100), unknown phase, and MA<sub>6</sub>PbI<sub>8</sub>·2MeOH (200) peak area (b) and Scherrer size (c) over one cycle of exposure to MeOH and 75 °C in panel a. (c) Two cycles of alternating exposure to MeOH and H<sub>2</sub>O vapor at room temperature. Comparison of MAI (100), MAPbI<sub>3</sub> (100), unknown phase, MA<sub>6</sub>PbI<sub>8</sub>·2MeOH (200), and MA<sub>4</sub>PbI<sub>6</sub>·2H<sub>2</sub>O (101) peak area (e) and Scherrer size (f) over two cycles of alternating exposure to MeOH and H<sub>2</sub>O vapor in panel c.

rapid conversion between methanolated and hydrated films (<30 s) relative to the process of methanolating or hydrating a colored film containing 3D MAPbI<sub>3</sub> and MAI (>1 min) suggests that exchanging MeOH/H<sub>2</sub>O has a smaller thermodynamic driving force than intercalating MeOH/H<sub>2</sub>O because the [PbI<sub>6</sub>]<sup>4-</sup> octahedra in the structures are already separated (Figure 1).

The structural transformations between 3D and 0D structures are accompanied by reversible optical coloration and bleaching. Optical absorption measurements show that switchable MHP films in the colored (heated) state exhibit strong visible absorbance with a band gap onset of 1.80 eV (Figure 3a), which is larger than the typical 1.57 eV band gap observed for MAPbI<sub>3</sub>.<sup>1</sup> Whereas our average MAPbI<sub>3</sub> domain size (36 ± 3 nm) is greater than the exciton Bohr radius,

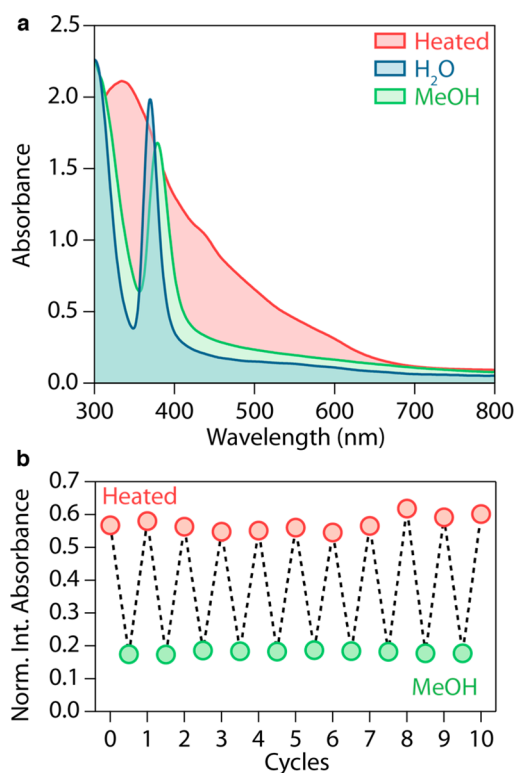


**Figure 3.** (a) Optical absorption of the same switchable MHP film exposed to MeOH, H<sub>2</sub>O, and heat. (b) Normalized integrated absorption over 10 cycles of alternating exposure to MeOH and 100 °C.

quantum confinement likely plays a role in the observed blueshift due to a population of smaller crystallites. Dielectric confinement likely also plays a role, since MAPbI<sub>3</sub> domains are surrounded by higher dielectric constant materials (Al<sub>2</sub>O<sub>3</sub>, TiO<sub>2</sub>, MAI). The largest contribution is likely scaffold-induced disorder with up to 70% of the material within a scaffold forming highly disordered phases with local MHP structure only extending over ~1.4 nm.<sup>32</sup>

Exposure to MeOH or H<sub>2</sub>O induces optical bleaching of the film in the visible region with the emergence of strong excitonic peaks at 379 and 370 nm, respectively. Heating methanolated and hydrated films above 50 and 70 °C, respectively, initiates complex dissociation resulting in the re-emergence of the 1.80 eV band gap and visible absorbance. The excitonic absorption peaks are due to absorption of the isolated [PbI<sub>6</sub>]<sup>4-</sup> octahedra formed upon intercalation of vapor. Hydrated and methanolated phases are readily interconverted accompanied by a shift in the peak absorbance ( $\lambda_{\text{max}}$ ) between 379 nm (methanolated) and 370 nm (hydrated) (Figure S5). The energy of the [PbI<sub>6</sub>]<sup>4-</sup> excitonic peak increases with more isolation and decreases with less isolation.<sup>33</sup> 0D MA<sub>6</sub>PbI<sub>8</sub>·2MeOH contains closely packed octahedra separated by only MAI with sheets of octahedra separated by both MeOH and MAI in the orthogonal direction. In contrast, 0D MA<sub>4</sub>PbI<sub>6</sub>·2H<sub>2</sub>O contains an isotropic 3D network of isolated octahedra separated by both MAI and H<sub>2</sub>O leading to an increased separation of isolated octahedra. The methanolated films also exhibit increased absorbance at wavelengths lower than 550 nm compared to hydrated films (Figure 3), which we attribute to formation of the unknown phase.

Durable, low-energy cycling between two optically distinct states is critical for a number of applications. We demonstrate reversible methanolation between two optically distinct states over 10 cycles to provide a glimpse of future application space (Figure 3b). Large swings in transmission are critical to building energy savings in thermochromic windows.<sup>34</sup> Optically active phase-change materials underpin memory applications with continued exploration of next-generation computing strategies such as on-chip photonic synapses.<sup>35</sup> Herein, we demonstrate a transition temperature less than conventional chalcogenide-based phase-change materials with similar optical contrast between states.

In conclusion, we show that MHPs form 0D intercalation complexes with MeOH driven by H-bonding between MeOH and the MHP lattice. MeOH within the 0D complex is reversibly exchanged for H<sub>2</sub>O by inducing a change in the chemical potential of the system through Le Chatelier's principle. The 0D complex can be dissociated to regenerate the 3D MHP structure by removing MeOH through mild heating above 50 °C. Our results demonstrate that weaker H-bonding reduces the switching temperature of switchable MHP films, thus enabling next-generation stimuli-responsive MHP applications that require low-energy modulation such as low-power-consumption memory, neuromorphic computing, switchable photovoltaics, and thermochromic windows.<sup>36</sup>

## ■ ASSOCIATED CONTENT

### Supporting Information

The Supporting Information is available free of charge at <https://pubs.acs.org/doi/10.1021/jacs.1c10942>.

Experimental details, additional optical photographs, ATR-FTIR spectra, WAXS peak identification, and optical absorption cycling spectral data (PDF)

## ■ AUTHOR INFORMATION

### Corresponding Author

Lance M. Wheeler – National Renewable Energy Laboratory, Golden, Colorado 80401, United States; [orcid.org/0000-0002-1685-8242](https://orcid.org/0000-0002-1685-8242); Email: lance.wheeler@nrel.gov

### Authors

Bryan A. Rosales – National Renewable Energy Laboratory, Golden, Colorado 80401, United States; [orcid.org/0000-0003-2488-7446](https://orcid.org/0000-0003-2488-7446)

Laura E. Mundt – SLAC National Accelerator Laboratory, Menlo Park, California 94025, United States; [orcid.org/0000-0003-4501-2374](https://orcid.org/0000-0003-4501-2374)

Laura T. Schelhas – National Renewable Energy Laboratory, Golden, Colorado 80401, United States; [orcid.org/0000-0003-2299-1864](https://orcid.org/0000-0003-2299-1864)

Complete contact information is available at: <https://pubs.acs.org/10.1021/jacs.1c10942>

### Notes

The authors declare no competing financial interest.

## ■ ACKNOWLEDGMENTS

This study was authored by the National Renewable Energy Laboratory, operated by Alliance for Sustainable Energy, LLC, for the U.S. Department of Energy (DOE) under Contract DE-AC36-08GO28308. Funding was provided by the Building Technologies Office within the U.S. Department of Energy

Office of Energy Efficiency and Renewable Energy. Use of the Stanford Synchrotron Radiation Lightsource, SLAC National Accelerator Laboratory, was supported by the U.S. Department of Energy, Office of Basic Energy Sciences, under Contract DE-AC02-76SF00515. The views expressed in the article do not necessarily represent the views of the DOE or the U.S. Government. The U.S. Government retains and the publisher, by accepting the article for publication, acknowledges that the U.S. Government retains a nonexclusive, paid-up, irrevocable, worldwide license to publish or reproduce the published form of this study, or allow others to do so, for U.S. Government purposes.

## ABBREVIATIONS

metal halide perovskite, MHP; methanol, MeOH; methylammonium, MA; *N,N*-dimethylformamide, DMF; oleylammonium, OA; wide-angle X-ray scattering, WAXS; attenuated total reflection Fourier transform infrared spectroscopy, ATR-FTIR; visible transmittance, VT; power conversion efficiency, PCE

## REFERENCES

- (1) Chouhan, L.; Ghimire, S.; Subrahmanyam, C.; Miyasaka, T.; Biju, V. Synthesis, Optoelectronic Properties and Applications of Halide Perovskites. *Chem. Soc. Rev.* **2020**, *49* (10), 2869–2885.
- (2) Dey, A.; Ye, J.; De, A.; Debroye, E.; Ha, S. K.; Bladt, E.; Kshirsagar, A. S.; Wang, Z.; Yin, J.; Wang, Y.; et al. State of the Art and Prospects for Halide Perovskite Nanocrystals. *ACS Nano* **2021**, *15* (7), 10775–10981.
- (3) Fu, Y.; Zhu, H.; Chen, J.; Hautzinger, M. P.; Zhu, X. Y.; Jin, S. Metal Halide Perovskite Nanostructures for Optoelectronic Applications and the Study of Physical Properties. *Nat. Rev. Mater.* **2019**, *4* (3), 169–188.
- (4) Leijtens, T.; Bush, K. A.; Prasanna, R.; McGehee, M. D. Opportunities and Challenges for Tandem Solar Cells Using Metal Halide Perovskite Semiconductors. *Nat. Energy* **2018**, *3* (10), 828–838.
- (5) Tennyson, E. M.; Doherty, T. A. S.; Stranks, S. D. Heterogeneity at Multiple Length Scales in Halide Perovskite Semiconductors. *Nat. Rev. Mater.* **2019**, *4* (9), 573–587.
- (6) Zou, C.; Zhang, C.; Kim, Y.-H.; Lin, L. Y.; Luther, J. M. The Path to Enlightenment: Progress and Opportunities in High Efficiency Halide Perovskite Light-Emitting Devices. *ACS Photon.* **2021**, *8* (2), 386–404.
- (7) Zhu, H.; Miyata, K.; Fu, Y.; Wang, J.; Joshi, P. P.; Niesner, D.; Williams, K. W.; Jin, S.; Zhu, X. Y. Screening in Crystalline Liquids Protects Energetic Carriers in Hybrid Perovskites. *Science* **2016**, *353* (6306), 1409–1413.
- (8) Manser, J. S.; Saidaminov, M. I.; Christians, J. A.; Bakr, O. M.; Kamat, P. V. Making and Breaking of Lead Halide Perovskites. *Acc. Chem. Res.* **2016**, *49* (2), 330–338.
- (9) Boyd, C. C.; Cheacharoen, R.; Leijtens, T.; McGehee, M. D. Understanding Degradation Mechanisms and Improving Stability of Perovskite Photovoltaics. *Chem. Rev.* **2019**, *119* (5), 3418–3451.
- (10) Best Research-Cell Efficiencies Chart. <https://www.nrel.gov/pv/cell-efficiency.html> (accessed Nov 21, 2021).
- (11) Rosales, B. A.; Mundt, L. E.; Allen, T. G.; Moore, D. T.; Prince, K. J.; Wolden, C. A.; Rumbles, G.; Schelhas, L. T.; Wheeler, L. M. Reversible Multicolor Chromism in Layered Formamidinium Metal Halide Perovskites. *Nat. Commun.* **2020**, *11* (1), 5234.
- (12) Wheeler, L. M.; Moore, D. T.; Ihly, R.; Stanton, N. J.; Miller, E. M.; Tenent, R. C.; Blackburn, J. L.; Neale, N. R. Switchable Photovoltaic Windows Enabled by Reversible Photochemical Complex Dissociation from Methylammonium Lead Iodide. *Nat. Commun.* **2017**, *8* (1), 1722.
- (13) Halder, A.; Choudhury, D.; Ghosh, S.; Subbiah, A. S.; Sarkar, S. K. Exploring Thermochromic Behavior of Hydrated Hybrid Perovskites in Solar Cells. *J. Phys. Chem. Lett.* **2015**, *6* (16), 3180–3184.
- (14) Fateev, S. A.; Petrov, A. A.; Khrustalev, V. N.; Dorovatovskii, P. V.; Zubavichus, Y. V.; Goodilin, E. A.; Tarasov, A. B. Solution Processing of Methylammonium Lead Iodide Perovskite from  $\gamma$ -Butyrolactone: Crystallization Mediated by Solvation Equilibrium. *Chem. Mater.* **2018**, *30* (15), 5237–5244.
- (15) Cao, J.; Jing, X.; Yan, J.; Hu, C.; Chen, R.; Yin, J.; Li, J.; Zheng, N. Identifying the Molecular Structures of Intermediates for Optimizing the Fabrication of High-Quality Perovskite Films. *J. Am. Chem. Soc.* **2016**, *138* (31), 9919–26.
- (16) Petrov, A. A.; Sokolova, I. P.; Belich, N. A.; Peters, G. S.; Dorovatovskii, P. V.; Zubavichus, Y. V.; Khrustalev, V. N.; Petrov, A. V.; Grätzel, M.; Goodilin, E. A.; Tarasov, A. B. Crystal Structure of DMF-Intermediate Phases Uncovers the Link Between  $\text{CH}_3\text{NH}_3\text{PbI}_3$  Morphology and Precursor Stoichiometry. *J. Phys. Chem. C* **2017**, *121* (38), 20739–20743.
- (17) Schaak, R. E.; Mallouk, T. E. Perovskites by Design: A Toolbox of Solid-State Reactions. *Chem. Mater.* **2002**, *14* (4), 1455–1471.
- (18) Dawson, J. A.; Naylor, A. J.; Eames, C.; Roberts, M.; Zhang, W.; Snaith, H. J.; Bruce, P. G.; Islam, M. S. Mechanisms of Lithium Intercalation and Conversion Processes in Organic-Inorganic Halide Perovskites. *ACS Energy Lett.* **2017**, *2* (8), 1818–1824.
- (19) Zhang, F.; Lu, H.; Tong, J.; Berry, J. J.; Beard, M. C.; Zhu, K. Advances in Two-Dimensional Organic-Inorganic Hybrid Perovskites. *Energy Environ. Sci.* **2020**, *13* (4), 1154–1186.
- (20) Mitzi, D. B.; Medeiros, D. R.; Malenfant, P. R. L. Intercalated Organic-Inorganic Perovskites Stabilized by Fluoroaryl-Aryl Interactions. *Inorg. Chem.* **2002**, *41* (8), 2134–2145.
- (21) Sharma, S. K.; Phadnis, C.; Das, T. K.; Kumar, A.; Kavaipatti, B.; Chowdhury, A.; Yella, A. Reversible Dimensionality Tuning of Hybrid Perovskites with Humidity: Visualization and Application to Stable Solar Cells. *Chem. Mater.* **2019**, *31* (9), 3111–3117.
- (22) Huisman, B. A. H.; Palazon, F.; Bolink, H. J. Zero-Dimensional Hybrid Organic-Inorganic Lead Halides and Their Post-Synthesis Reversible Transformation into Three-Dimensional Perovskites. *Inorg. Chem.* **2021**, *60*, 5212–5216.
- (23) Liu, S.; Du, Y. W.; Tso, C. Y.; Lee, H. H.; Cheng, R.; Feng, S. P.; Yu, K. M. Organic Hybrid Perovskite ( $\text{MAPbI}_{3-x}\text{Cl}_x$ ) for Thermochromic Smart Window with Strong Optical Regulation Ability, Low Transition Temperature, and Narrow Hysteresis Width. *Adv. Funct. Mater.* **2021**, *31*, 2010426.
- (24) Zhang, Y.; Tso, C. Y.; Inigo, J. S.; Liu, S.; Miyazaki, H.; Chao, C. Y. H.; Yu, K. M. Perovskite Thermochromic Smart Window: Advanced Optical Properties and Low Transition Temperature. *Appl. Energy* **2019**, *254*, 113690.
- (25) Koutselas, I. B.; Ducasse, L.; Papavassiliou, G. C. Electronic Properties of Three- and Low-Dimensional Semiconducting Materials with Pb Halide and Sn Halide Units. *J. Phys. Cond. Matter* **1996**, *8* (9), 1217–1227.
- (26) Vincent, B. R.; Robertson, K. N.; Cameron, T. S.; Knop, O. Alkylammonium Lead Halides. Part 1. Isolated  $\text{PbI}_6^{4-}$  Ions in  $(\text{CH}_3\text{NH}_3)_4\text{PbI}_6 \cdot 2\text{H}_2\text{O}$ . *Can. J. Chem.* **1987**, *65* (5), 1042–6.
- (27) Lin, J.; Lai, M.; Dou, L.; Kley, C. S.; Chen, H.; Peng, F.; Sun, J.; Lu, D.; Hawks, S. A.; Xie, C.; Cui, F.; Alivisatos, A. P.; Limmer, D. T.; Yang, P. Thermochromic Halide Perovskite Solar Cells. *Nat. Mater.* **2018**, *17* (3), 261–267.
- (28) Yang, F.; Kamarudin, M. A.; Zhang, P.; Kapil, G.; Ma, T.; Hayase, S. Enhanced Crystallization by Methanol Additive in Antisolvent for Achieving High-Quality  $\text{MAPbI}_3$  Perovskite Films in Humid Atmosphere. *ChemSusChem* **2018**, *11* (14), 2348–2357.
- (29) Acik, M.; Alam, T. M.; Guo, F.; Ren, Y.; Lee, B.; Rosenberg, R. A.; Mitchell, J. F.; Park, I. K.; Lee, G.; Darling, S. B. Substitutional Growth of Methylammonium Lead Iodide Perovskites in Alcohols. *Adv. Energy Mater.* **2018**, *8* (5), 1701726.
- (30) Liu, X.; Luo, Z.; Yin, W.; Litvin, A. P.; Baranov, A. V.; Zhang, J.; Liu, W.; Zhang, X.; Zheng, W. Methanol-Induced Fast CsBr Release

Results in Phase-Pure CsPbBr<sub>3</sub> Perovskite Nanoplatelets. *Nanoscale Adv.* **2020**, *2* (5), 1973–1979.

(31) Liu, C.; Wang, K.; Yi, C.; Shi, X.; Smith, A. W.; Gong, X.; Heeger, A. J. Efficient Perovskite Hybrid Photovoltaics via Alcohol-Vapor Annealing Treatment. *Adv. Funct. Mater.* **2016**, *26* (1), 101–110.

(32) Choi, J. J.; Yang, X.; Norman, Z. M.; Billinge, S. J.; Owen, J. S. Structure of Methylammonium Lead Iodide Within Mesoporous Titanium Dioxide: Active Material in High-Performance Perovskite Solar Cells. *Nano Lett.* **2014**, *14* (1), 127–133.

(33) Thumu, U.; Piotrowski, M.; Owens-Baird, B.; Kolen'ko, Y. V. Zero-Dimensional Cesium Lead Halide Perovskites: Phase Transformations, Hybrid Structures, and Applications. *J. Solid State Chem.* **2019**, *271*, 361–377.

(34) Long, L.; Ye, H. How to be Smart and Energy Efficient: A General Discussion on Thermochromic Windows. *Sci. Rep.* **2015**, *4*, 6427.

(35) Cheng, Z.; Ríos, C.; Pernice, W. H. P.; Wright, C. D.; Bhaskaran, H. On-Chip Photonic Synapse. *Sci. Adv.* **2017**, *3* (9), No. e1700160.

(36) Zhumekenov, A. A.; Saidaminov, M. I.; Mohammed, O. F.; Bakr, O. M. Stimuli-Responsive Switchable Halide Perovskites: Taking Advantage of Instability. *Joule* **2021**, *5* (8), 2027–2046.



ACS IN FOCUS

Cellular Agriculture: Lab-Grown  
Dilek Erilliç, Corinna Dorothea

Machine Learning in Chemistry  
Jon Paul Janet & Heather J. Kulik

bacterials  
Teresa Cheng Jaramillo, William M. Wuest

ACS In Focus ebooks are digital publications that help readers of all levels accelerate their fundamental understanding of emerging topics and techniques from across the sciences.

pubs.acs.org/series/infocus

ACS Publications  
Most Trusted. Most Cited. Most Read.

<https://doi.org/10.1021/jacs.1c10942>